

# Skeletal Cubic, Lamellar, and Ribbon Phases of Bundled Thermotropic Bolapolyphiles

Feng Liu,<sup>\*,†,‡,§</sup> Marko Prehm,<sup>||,§</sup> Xiangbing Zeng,<sup>‡</sup> Carsten Tschierske,<sup>\*,||</sup> and Goran Ungar<sup>\*,‡,⊥</sup>

<sup>†</sup>State Key Laboratory for Mechanical Behavior of Materials, Xi'an Jiaotong University, Xi'an 710049, P. R. China

<sup>‡</sup>Department of Materials Science and Engineering, University of Sheffield, Mappin Street, Sheffield S1 3JD, U.K.

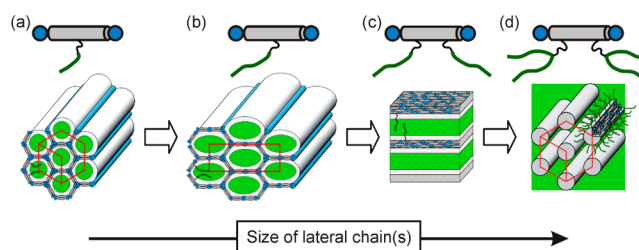
<sup>||</sup>Institute of Chemistry, Organic Chemistry, Martin-Luther-University Halle-Wittenberg, D-06120 Halle, Germany

<sup>⊥</sup>Department of Physics, Zhejiang Sci-Tech University, Xiasha College Park, Hangzhou 310018, P. R. China

## Supporting Information

**ABSTRACT:** A series of T-shaped polyphilic molecules composed of a rigid linear biphenyl core with a polar glycerol group at each end and one swallow-tail semi-perfluorinated lateral chain were synthesized and their thermotropic liquid crystalline (LC) phases were investigated by X-ray diffraction, calorimetry, and microscopy. The compounds have a long alkyl spacer between the aromatic core and the fluorinated  $C_nF_{2n+1}$  ends, where  $n = 4, 6, 8,$  and  $10$ . Upon melting, all compounds start with lamellar LC phases, followed on heating by a rectangular columnar ribbon phase with  $c2mm$  symmetry. Unusually, a ribbon is a flat bundle of molecular cores highly aligned *parallel* to the ribbon axis. On further heating, for  $n = 8$  and  $10$ , this phase is succeeded by a bicontinuous cubic phase with  $Ia\bar{3}d$  symmetry. This is a new variant of the “gyroid” phase, with axially oriented rod-like molecular cores forming the skeleton of the two infinite networks and junctions separated by exactly two molecular lengths. In this tricontinuous core–shell structure (aromatic–aliphatic–perfluoroalkyl), the polar glycerol domains of appreciable size, contained within the skeleton, can be considered as micellar.

Rod-like amphiphiles with laterally attached flexible chains display a large variety of thermotropic liquid crystalline (LC) phases, foremost of which are honeycomb phases made up of cylinders with different polygonal cross sections.<sup>1,2</sup> The most representative group of compounds forming these phases are bolapolyphiles having a rod-like core, with a glycerol group at each end. The side chains, usually *n*-alkyl, semiperfluoroalkyl, or carbosilane, fill the interior of the polygonal cylinders. The walls are assembled from the aromatic rods lying normal to the cylinder axis and linked by the H-bonding glycerols. For small side chains, polygons could be triangles, rhombi, or squares, and pentagons or hexagons may be found for larger chains (Figure 1a). In all the above cases, the side of the polygon is one molecule long, but there are instances where the side contains two rods linked end-to-end, as in the example of stretched or “giant” hexagons (Figure 1b),<sup>3</sup> or in the recently reported complex honeycomb consisting of giant squares and octagons.<sup>4</sup> The complexity increases when two chains are attached to the opposite sides of the rod and, in particular, if



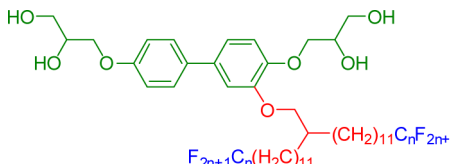
**Figure 1.** Sequence of LC phase types formed by rod-like bolapolyphiles with incompatible lateral and terminal groups, as seen upon increasing the size of the lateral chain(s) relative to the rod length: (a,b) polygonal cylinder phases (rods normal to column),<sup>1,3</sup> (c) Lam phases (rods in plane of layer),<sup>6–8</sup> and (d) axial-bundle phases (bundles of rods parallel to column).<sup>9,10</sup> Molecules displaying these phases are sketched above: gray = aromatic, blue = glycerol, black-green = side chain.

they are incompatible; that can result in “multicolor” honeycombs in which different cells contain different side chains, or different mixtures thereof.<sup>5</sup> However, it was found that if the total side chain volume exceeds a certain threshold, then the honeycomb arrangement becomes unsustainable, and the discrete cylinders merge into a continuous flat layer (Figure 1c).<sup>3,6–8</sup> In contrast to the usual layered smectic LCs, in these lamellar (Lam) phases the rod-like mesogens lie *parallel* to the plane of the layers.

If the side chain volume is increased still further, e.g., if the two linear chains in Figure 1c are replaced by one or two branched “swallow-tail” chains (Figure 1d), then a new class of columnar LC phases is obtained that can be considered as inverted honeycombs, with the rigid cores now in the center of the cylinders and the side chains at the periphery.<sup>9,10</sup> This type of arrangement is in fact more akin to the classic columnar phases of disk-shaped, slice-shaped, or polycatenar rod-like mesogens,<sup>1,11–13</sup> except that in the columnar bolapolyphiles the long molecular axis is *parallel* rather than normal to the column axis, and the rods are bunched together in bundles of about 10 (the “axial bundle” phases).<sup>9,10</sup> In a simplistic representation, the overall behavior described can be compared to that of lyotropic LCs, whereby the aromatic moieties represent water and the side chains represent the hydrophobic chains. The

Received: March 10, 2014

Published: April 21, 2014

Table 1. Transition Temperatures and Lattice Parameters<sup>a</sup>


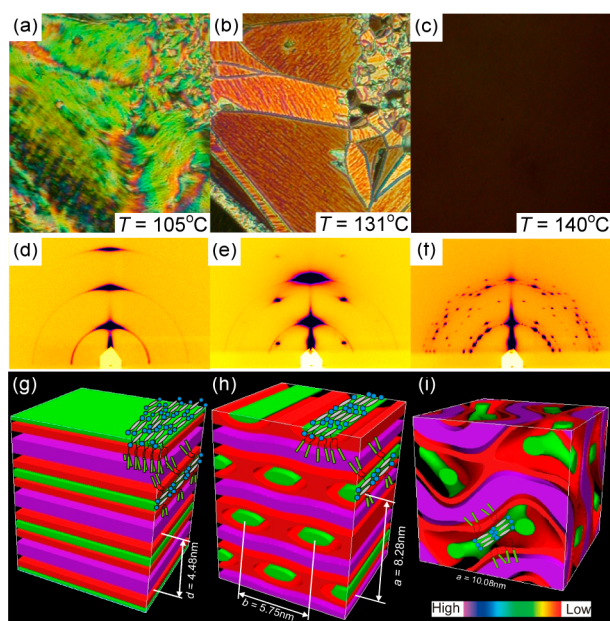
compd	<i>n</i>	<i>T</i> /°C	lattice parameter/nm
1/4	4	Cr 60 Lam <sub>Sm</sub> 129 Iso	<i>d</i> = 3.68
1/6	6	Cr 57 Lam <sub>Sm</sub> 119 Lam <sub>N</sub> 125 Col <sub>rec</sub> / <i>c2mm</i> 131 Iso	<i>d</i> = 4.04 <i>a</i> = 7.64, <i>b</i> = 4.91
1/8	8	Cr 75 Lam <sub>Sm</sub> 102 Lam <sub>N</sub> 106 Col <sub>rec</sub> / <i>c2mm</i> 132 Cub/ <i>Ia3d</i> 154 Iso	<i>d</i> = 4.48 <i>a</i> = 8.28, <i>b</i> = 5.75 <i>a</i> <sub>cub</sub> = 10.08
1/10	10	Cr 108 Lam <sub>Sm</sub> 132 Lam <sub>N</sub> 133 Col <sub>rec</sub> / <i>c2mm</i> 145 Cub/ <i>Ia3d</i> 178 Iso	<i>d</i> = 5.15 <i>a</i> = 9.02, <i>b</i> = 6.14 <i>a</i> <sub>cub</sub> = 10.80

<sup>a</sup>From first DSC heating (10 K min<sup>-1</sup>) and POM; Cr, crystalline; Lam<sub>Sm</sub>, lamellar smectic; Lam<sub>N</sub>, lamellar nematic; Col<sub>rec</sub>/*c2mm*, rectangular *c2mm*; Cub/*Ia3d*, gyroid cubic; Iso, isotropic liquid. For transition enthalpies see Table S1.

honeycomb–Lam–axial bundle phase sequence can then be compared to the lyotropic sequence, direct hexagonal–lamellar–inverse hexagonal, as the hydrophobic fraction increases (water fraction decreases). As is well known, in the lyotropic range between lamellar and hexagonal phases, several “intermediate” phases may appear, of which the bicontinuous cubic (Cub<sub>bi</sub>) phases are best known.<sup>14</sup> It is tempting to ask whether an equivalent intermediate phase can be found also in the thermotropic bolopolyphiles. Several examples of the double gyroid Cub<sub>bi</sub> phase have been found in thermotropic LCs, mostly in the “polycatenar” rod-like compounds bearing between one and three terminally attached chains.<sup>15–18</sup> In this Communication we indeed report, for the first time, two thermotropic intermediate phases in laterally substituted bolopolyphiles. While they share a number of geometrical features with the intermediate phases in lyotropic and polycatenar systems, as will be shown, the molecular organization is quite different.

Compounds 1/*n* investigated in this work contain a symmetric “swallow-tail” lateral group, with a  $-(\text{CH}_2)_{11}$ -spacer and a perfluorinated end-segment,  $-\text{C}_n\text{F}_{2n+1}$ , in each branch (see Table 1). Details of the synthesis are given in the Supporting Information (SI). The compounds were investigated by polarized optical microscopy (POM), differential scanning calorimetry (DSC), powder X-ray diffraction (XRD), and grazing-incidence small-angle X-ray scattering (GISAXS) on thin surface-aligned films on glass or silicon. For selected compounds synchrotron radiation was used. Electron density (ED) maps were reconstructed using powder XRD intensities. For details of experiments and analysis, see SI.2

Phase transition temperatures and associated enthalpy values are collated in Tables 1 and S1, respectively. All compounds display broad regions of enantiotropic (reversible) LC phases. As expected, in the LC temperature range the XRD patterns show only diffuse wide-angle scattering (e.g., maximum at *d* = 0.56 nm for 1/10, see Figure S9f). Indexing of the small-angle Bragg reflections (see Tables S2–S10 and Figures S10–S12) led to the phase assignments, plane and space groups shown in Table 1.

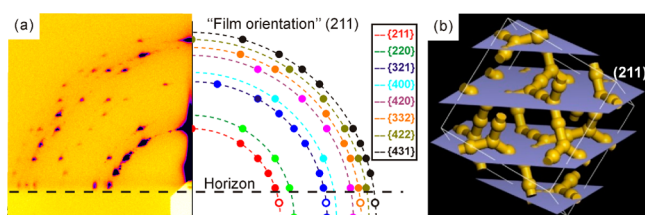


**Figure 2.** Compound 1/8. (a–c) Texture as seen between crossed polarizers in (a) the Lam<sub>N</sub> phase at *T* = 105 °C; (b) the Col<sub>rec</sub>/*c2mm* phase at *T* = 131 °C; and (c) the Cub/*Ia3d* phase at *T* = 140 °C. (d–f) GISAXS patterns of (d) Lam<sub>Sm</sub> at *T* = 100 °C, (e) Col<sub>rec</sub>/*c2mm* at *T* = 110 °C; and (f) Cub/*Ia3d* at *T* = 140 °C. For indexing see Figure S13. (g–i) Histogrammatic electron density maps with added schematic molecules for (g) Lam, (h) Col<sub>rec</sub>/*c2mm*, and (i) Cub/*Ia3d*. For simplicity, discrete solid colors are allocated to three different ED ranges, purple for the highest, green for the middle, and red for the lowest; they correspond roughly to chemical group colors in Table 1. The continuous color scale is shown underneath panel (i); intermediate density ranges (yellow, blue) were cut out in order to visualize the cell interior.

As typically observed for T-shaped polyphiphiles with large lateral substituents,<sup>1,6–8</sup> all four compounds display lamellar phases at lower temperatures. This is illustrated for compound 1/8 by the GISAXS pattern in Figure 2d. A series of strong Bragg reflections with associated *d*-spacings of 4.48, 2.25, and 1.50 nm, ratio 1:<sup>1</sup>/<sub>2</sub>:<sup>1</sup>/<sub>3</sub>, are seen along the meridian. This implies layers parallel to the (horizontal) substrate (see also Figures S8a and S9a). At the same time, the sample shows strong birefringence (Figure 2a; see also Figures S5 and S6), consistent with the aromatic rods lying in the layer plane, as is typical for the Lam phases in T-shaped bolopolyphiles and unlike in conventional smectics. The observed lattice parameters increase with increasing length of the lateral chains (see Table 1).

From powder XRD intensities we obtained a 1D electron density profile along the layer normal, shown as a 3D color map in Figure 2g. As shown by the superimposed schematic molecules, the aromatic double-layer (green) is surrounded on both sides by a layer of aliphatic spacers (lowest density, red) followed by a fluorocarbon double-layer (highest density, purple; see the predicted electron densities for the aromatic, aliphatic, and perfluoroalkyl regions in Table S13). There is positional order of the aromatic mesogens within the aromatic layer plane in the Lam<sub>Sm</sub> phase (*T* < 102 °C for 1/8, Table 1), whereas in the Lam<sub>N</sub> phase (*T* > 102 °C) the mesogens are positionally disordered, giving a 2D nematic.

At higher temperatures all compounds except 1/4 transform to a centered rectangular columnar phase, plane group *c2mm*, as



**Figure 3.** (a) Experimental and simulated GISAXS patterns of the  $Ia\bar{3}d$  phase of 1/8. Spots of different colors belong to different reflection groups (see legend). Simulated spots within a group are generated by permutation of  $\{hkl\}$  indices while keeping one of the  $\{211\}$  planes horizontal. Solid circles, observed; open circles, hidden below horizon. (b) Model of the infinite networks in an  $Ia\bar{3}d$  unit cell intersected by horizontal (211) planes.

shown by the additional  $hk$  diffraction spots on “half” layer lines (Figure 2e; also Figures S8c and S9c). The indices, experimental and calculated  $d$ -spacings, diffraction intensities, and phase angles of the  $Col_{rec}/c2mm$  phase of compound 1/8 are listed in Table S6. In the ED map in Figure 2h, reconstructed using these intensities and phases, it is evident that the continuous aromatic layers of the Lam phase break up into ribbons, while the fluoroalkyl layers become slightly wavy (see also maps in Figure S14). The Lam– $Col_{rec}$  transition is believed to be the result of the thermal expansion of the side chains requiring a positive mean curvature of the aromatic–aliphatic interface. The use of POM with  $\lambda$ -plate confirmed that the rod-like cores are parallel to the ribbon axis (see Figure S5c). According to volume calculation, a flat ribbon in 1/8 contains a bundle of 24 molecules in cross section (Table S11). The orientation of the director remains mainly unchanged upon the transition, as seen from optical micrographs in Figure 2a,b; only the smoothly curving director field of the Lam<sub>N</sub> phase gives way to sharp breaks at grain boundaries of the  $Col_{rec}$  phase, indicating a greatly increased bend modulus. Unusually for a transition on heating, the orientational order parameter *increases* in the  $Col_{rec}$  phase, as judged by the change in color from yellow-green to orange (Figures 2a,b and explanation in SI). This can be understood as the highly oriented  $Col_{rec}$  ribbons acting as nanochannels, confining the mesogenic cores within to lie along the channel axis.

At still higher temperatures, compounds 1/8 and 1/10 transform to an optically isotropic LC phase (Figure 2c). The small-angle powder diffraction patterns show a number of sharp reflections (Figures S11b and S12c), their reciprocal spacings being in the ratio  $6^{1/2}:8^{1/2}:14^{1/2}:16^{1/2}:20^{1/2}:22^{1/2}:24^{1/2}:26^{1/2}$ , conforming to a cubic phase with  $Ia\bar{3}d$  symmetry. The GISAXS pattern of a highly aligned film of 1/8 is shown in Figures 2f and 3a. In Figure 3a it is juxtaposed against a simulated pattern based on fiber-type orientation, with  $[211]$ , as the unique axis, perpendicular to the substrate. Spots with different colors represent different  $\{hkl\}$  reflection groups. Thirteen layer lines of fiber diffraction are visible. The simulated and experimental patterns are in excellent agreement.

The reconstructed ED map of the  $Cub/Ia\bar{3}d$  phase of compound 1/8, which was obtained using the corrected diffraction intensities and structure factor phase angles (0 or  $\pi$ ) listed in Table S7, is shown in Figure 2i. The high-density purple regions contain the fluorinated segments of the semiperfluorinated lateral chains and are centered around the infinite periodic minimal gyroid (G) surface, characteristic of this “double gyroid” structure.<sup>19</sup> The green medium-density

branched networks contain the aromatic cores and glycerol groups, while the lowest density red regions interposed between the above two contain mainly the aliphatic spacers. EDs and volume fractions calculated from molecular models are listed in Table S13. The electron density histogram of the  $Cub/Ia\bar{3}d$  phase, supporting the chosen phase combination, is shown in Figure S15. We note that, while in most reported cases maximum and minimum ED regions are the continuous networks and the continuous G-surface, respectively,<sup>15,20</sup> in the current “tricontinuous” structure the minimum density continuum is intercalated between the two.

Based on the lattice parameter, the distance between two junctions of the network is 3.56 nm. This is twice the molecular length,  $L = 1.80$  nm, measured between the diol ends. Accordingly, we suggest that each network segment contains two successive coaxial bundles of molecules (Figure 2i). Based on the volumes of a molecule and the unit cell, there are  $\sim 566$  molecules per cell. As there are 24 network segments or 48 bundles per cell, each bundle contains 12 molecules on average, half the number in a  $Col_{rec}$  ribbon (compare Tables S11 and S12).

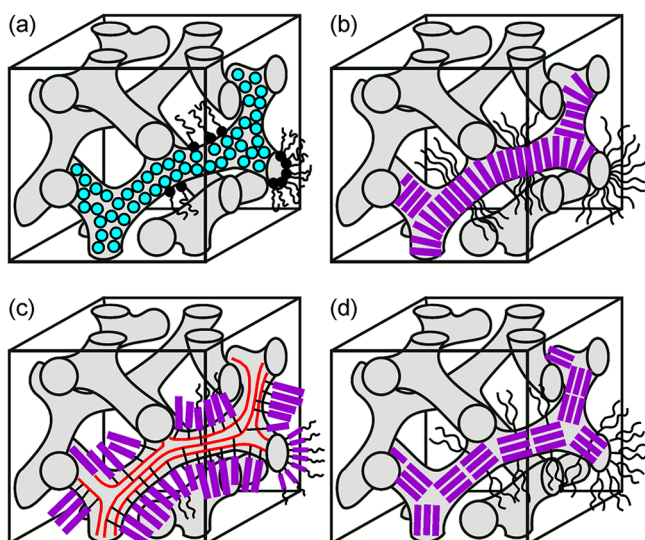
Furthermore, the closest distance between the two infinite networks is  $a \times 3^{1/2} / 4 = 4.37$  nm, half that value (2.2 nm) being the distance from the network to the minimal surface. This is slightly shorter than an extended lateral chain ( $\sim 2.50$  nm), so there is no problem for the chains to reach the minimal surface and fill the space of the cubic cell.

As can be seen in Figure 3a, all cubic domains lie with a  $\{211\}$  plane facing the substrate; no other orientation is observed. This is explained in Figure 3b: more than half of the network segments can be made to lie in a  $\{211\}$  plane with little distortion. Thus, cropping the network along a  $\{211\}$  plane requires the least distortion and the lowest number of “broken bonds”, while allowing most of the polar glycerol-based hydrogen-bonding clusters to stay in contact with the oxidized Si surface. Incidentally, it is no coincidence that the contact plane, a densely packed plane with high-amplitude ED modulation along its normal, is also the strongest diffracting plane (see Figure 3a), as often found in such systems.<sup>21,22</sup>

Referring to the scheme in Figure 1, we can now insert two new phases between the Lam (c) and axial bundle  $Col_h$  phases (d): the  $Col_{rec}/c2mm$  ribbon phase (Figure 2h) and what we may call the “skeletal” bicontinuous gyroid  $Cub/Ia\bar{3}d$  phase (Figure 2i). Ribbon<sup>23</sup> and  $Cub_{bi}$  phases<sup>14</sup> are two alternative solutions when the required interface curvature is too high for flat layers and too low for circular columns ( $Col_h$ ).<sup>19</sup> However, instances of the two phases occurring successively in the same system are quite rare. As shown above, the number of molecules side-by-side in a  $Col_{rec}$  bundle (24) is twice that in a  $Cub_{bi}$  bundle (12). One can ask why a larger  $Cub_{bi}$  structure, with thicker bundles containing 24 molecules, did not form instead of the  $Col_{rec}$  phase. The likely answer is that all molecules must reside at the surface of the bundle to allow their side chain access to the non-aromatic continuum. For circular bundles with 24 molecules this is impossible, hence the flat bundles of the  $Col_{rec}$  phase. At higher temperatures the necessary mean curvature increases, stabilizing thinner bundles and allowing them to be closer to circular, as required by the  $Cub_{bi}$  geometry.

Finally, the current  $Cub/Ia\bar{3}d$  phase is the first example where the mesogen long axis lies along the axis of the network segments, creating a relatively rigid skeleton with flexible H-bonded hinges. Such an arrangement imposes the extra





**Figure 4.** Double network structure of the  $Ia\bar{3}d$  cubic phase with schematic representation of molecules forming it in some LC systems of different types: (a) inverse lyotropic  $V_{II}$  phase with water in the channels,<sup>14</sup> (b) widely reported polycatenar thermotropic LCs,<sup>15–18</sup> (c) a polysiloxane with hemiphasmid polycatenar side groups,<sup>24</sup> and (d) the current skeletal network structure of H-bonded axial mesogen bundles.

constraint of interjunction distance being confined to an integer number of molecular lengths. This new assembly mode can be considered the fourth type of  $Cub_{bi}$  LC phases (Figure 4d), alongside the lyotropic case (Figure 4a), thermotropic phases with rod, disc, or fan-shaped mesogens all lying perpendicular to the network channel (Figure 4b),<sup>13,15,20</sup> and a reported case of a polymer with polysiloxane backbones in the channels and the rod-like side groups in the surrounding continuum (Figure 4c).<sup>24</sup> Thus, the present work expands the scope of the recently discovered family of axial bundle mesophases.<sup>9,10</sup> Furthermore, the polyphilic molecular structure (aromatic, aliphatic, fluororous, and polar segments) is shown to result in LC phases of increased structural complexity.<sup>25</sup> The segregation between the rigid cores and flexible chains provides the double gyroid skeleton, and the hydrocarbon–fluorocarbon segregation leads to a tricontinuous core–shell structure. Moreover, the polar glycerol domains of appreciable size, contained within the skeleton, can be considered as micellar (Figures 2i and 3b). Overall, the present findings offer a source of new diversity in soft 3D self-assembly and in controlling electro-optical properties.

## ■ ASSOCIATED CONTENT

### Supporting Information

Experimental procedures with complete spectral and structural analysis. This material is available free of charge via the Internet at <http://pubs.acs.org>.

## ■ AUTHOR INFORMATION

### Corresponding Authors

feng.liu@mail.xjtu.edu.cn

carsten.tschierske@chemie.uni-halle.de

g.ungar@sheffield.ac.uk

### Author Contributions

<sup>§</sup>F.L. and M.P. contributed equally.

## Notes

The authors declare no competing financial interest.

## ■ ACKNOWLEDGMENTS

This work was supported by the National Natural Science Foundation of China (No. 21374086), the NSF-EPSRC PIRE program RENEW (EP/K034308/1), DFG (FG 1145, TS 39/21-2), and the Leverhulme Foundation (RPG-2012-804). For help with synchrotron experiments we thank Drs. Nick Terrill and Jen Hiller (I22) at Diamond, Drs. Xiuhong Li and Feng Tian (BL16B1) at SSRF, and Drs. Oier Bikondoa, Simon Brown, and Paul Thompson (BM28-XMaS) at ESRF.

## ■ REFERENCES

- (1) Tschierske, C. *Chem. Soc. Rev.* **2007**, *36*, 1930.
- (2) Ungar, G.; Tschierske, C.; Abetz, V.; Holyst, R.; Bates, M. A.; Liu, F.; Prehm, M.; Kieffer, R.; Zeng, X.; Walker, M.; Glettner, B.; Zywockinski, A. *Adv. Funct. Mater.* **2011**, *21*, 1296.
- (3) Prehm, M.; Liu, F.; Baumeister, U.; Zeng, X.; Ungar, G.; Tschierske, C. *Angew. Chem., Int. Ed.* **2007**, *46*, 7972.
- (4) Liu, F.; Kieffer, R.; Zeng, X.; Pelz, K.; Prehm, M.; Ungar, G.; Tschierske, C. *Nat. Commun.* **2012**, *3*, 1104.
- (5) Zeng, X. B.; Kieffer, R.; Glettner, B.; Nürnberger, C.; Liu, F.; Pelz, K.; Prehm, M.; Baumeister, U.; Hahn, H.; Lang, H.; Gehring, G. H.; Weber, C. H. M.; Hobbs, J. K.; Tschierske, C.; Ungar, G. *Science* **2011**, *331*, 1302.
- (6) Cheng, X. H.; Das, M. K.; Diele, S.; Tschierske, C. *Angew. Chem., Int. Ed.* **2002**, *41*, 4031.
- (7) Patel, N. M.; Syed, I. M.; Rosenblatt, C.; Prehm, M.; Tschierske, C. *Liq. Cryst.* **2005**, *32*, 55.
- (8) Prehm, M.; Cheng, X. H.; Diele, S.; Das, M. K.; Tschierske, C. *J. Am. Chem. Soc.* **2002**, *124*, 12072.
- (9) Prehm, M.; Liu, F.; Zeng, X.; Ungar, G.; Tschierske, C. *J. Am. Chem. Soc.* **2011**, *133*, 4906.
- (10) Liu, F.; Prehm, M.; Zeng, X.; Ungar, G.; Tschierske, C. *Angew. Chem., Int. Ed.* **2011**, *50*, 10599.
- (11) Chandrasekhar, S.; Sadashiva, B. K.; Suresh, K. A. *Pramana* **1977**, *9*, 471.
- (12) Percec, V.; Lee, M.; Heck, J.; Blackwell, H. E.; Ungar, G.; Alvarez-Castillo, A. *J. Mater. Chem.* **1992**, *2*, 931.
- (13) Malthête, J.; Levelut, A. M.; Nguyen, H. L. *J. Phys., Lett.* **1985**, *46*, 875.
- (14) Gruner, S. M. *J. Phys. Chem.* **1989**, *93*, 7562.
- (15) Levelut, A. M.; Clerc, M. *Liq. Cryst.* **1998**, *24*, 105.
- (16) Kutsumizu, S. *Curr. Opin. Solid State Mater. Sci.* **2002**, *6*, 537.
- (17) Alam, M. A.; Motoyanagi, J.; Yamamoto, Y.; Fukushima, T.; Kim, J.; Kato, K.; Takata, M.; Saeki, A.; Seki, S.; Tagawa, S.; Aida, T. *J. Am. Chem. Soc.* **2009**, *131*, 17722.
- (18) Chvalun, S. N.; Shcherbina, M. A.; Yakunin, A. N.; Blackwell, J.; Percec, V. *Polym. Sci. Ser. A* **2007**, *49*, 158.
- (19) Scriven, L. E. *Nature* **1976**, *263*, 123.
- (20) Ichikawa, T.; Yoshio, M.; Hamasaki, A.; Taguchi, S.; Liu, F.; Zeng, X. B.; Ungar, G.; Ohno, H.; Kato, T. *J. Am. Chem. Soc.* **2012**, *134*, 2634.
- (21) Weber, C. H. M.; Liu, F.; Zeng, X.-b.; Ungar, G.; Mullin, N.; Hobbs, J. K.; Jahr, M.; Lehmann, M. *Soft Matter* **2010**, *6*, 5390.
- (22) Ungar, G.; Liu, F.; Zeng, X. B.; Glettner, B.; Prehm, M.; Kieffer, R.; Tschierske, C. *J. Phys.: Conf. Ser.* **2010**, *247*, 012032.
- (23) Weber, P.; Guillon, D.; Skoulios, A.; Miller, R. D. *Liq. Cryst.* **1990**, *8*, 825.
- (24) Ungar, G.; Percec, V. Presented at the 14th International Liquid Crystal Conference, Pisa, Italy, 1992.
- (25) Tschierske, C. *Angew. Chem., Int. Ed.* **2013**, *52*, 8828.